A non-overlapping domain decomposition method with high-order transmission conditions and cross-point treatment for Helmholtz problems

Axel Modave, Anthony Royer, Xavier Antoine, Christophe Geuzaine

A non-overlapping domain decomposition method with high-order transmission conditions and cross-point treatment for Helmholtz problems*

A. Modave[1], A. Royer[3], X. Antoine[2], and C. Geuzaine[3]

[1]POEMS, CNRS, Inria, ENSTA Paris, Institut Polytechnique de Paris, 91120 Palaiseau (France), axel.modave@ensta-paris.fr
[2]Institut Elie Cartan de Lorraine, Université de Lorraine, Inria Nancy-Grand Est, EPI SPHINX, 54506 Vandoeuvre-lès-Nancy Cedex (France), xavier.antoine@univ-lorraine.fr
[3]Université de Liège, Institut Montefiore B28, 4000 Liège (Belgium), anthony.royer@uliege.be, cgeuzaine@uliege.be

Abstract

A non-overlapping domain decomposition method (DDM) is proposed for the parallel finite-element solution of large-scale time-harmonic wave problems. It is well-known that the convergence rate of this kind of method strongly depends on the transmission condition enforced on the interfaces between the subdomains. Local conditions based on high-order absorbing boundary conditions (HABCs) have proved to be well-suited, as a good compromise between basic impedance conditions, which lead to suboptimal convergence, and conditions based on the exact Dirichlet-to-Neumann (DtN) map related to the complementary of the subdomain — which are too expensive to compute. However, a direct application of this approach for configurations with interior cross-points (where more than two subdomains meet) and boundary cross-points (points that belong to both the exterior boundary and at least two subdomains) is suboptimal and, in some cases, can lead to incorrect results.

In this work, we extend a non-overlapping DDM with HABC-based transmission conditions approach to efficiently deal with cross-points for lattice-type partitioning. We address the question of the cross-point treatment when the HABC operator is used in the transmission condition, or when it is used in the exterior boundary condition, or both. The proposed cross-point treatment relies on corner conditions developed for Padé-type HABCs. Two-dimensional numerical results with a nodal finite-element discretization are proposed to validate the approach, including convergence studies with respect to the frequency, the mesh size and the number of subdomains. These results demonstrate the efficiency of the cross-point treatment for settings with regular partitions and homogeneous media. Numerical experiments with distorted partitions and smoothly varying heterogeneous media show the robustness of this treatment.

1 Introduction

The efficient and accurate finite element solution of high-frequency time-harmonic wave problems, such as scattering and wave propagation problems, remains a challenging issue in computational engineering. Indeed, first, the unbounded domain must be truncated, which requires a specific treatment to simulate the outward propagation of outgoing waves. Then, the discretization of formulations related to Helmholtz-type problems leads to very large, complex and indefinite (dense or sparse) linear systems, especially in the high-frequency regime, corresponding to the situation where the wavelength is small compared with the characteristic size of the scatterer.

Various approaches have been designed for solving high-frequency scattering problems. Among the most popular ones, the boundary element method (BEM) based on the discretization of a boundary integral equation [19, 63], in conjunction with a preconditioned Krylov subspace iterative solver [1, 20]

*Published in *Computer Methods in Applied Mechanics and Engineering*.

and fast compression algorithms of integral kernels [15, 16, 67], is a first direction. An alternative for engineering applications is to introduce a boundary condition on a fictitious surface or an absorbing boundary layer enclosing the scatterer to truncate the domain and then to discretize the associated variational formulation in the bounded volume domain *e.g.* using a finite element method (FEM). Many possibilities exist to bound the computational domain. Basically, there is always a trade-off between accuracy and computational effort when choosing one of the truncation strategies. The most basic absorbing boundary condition (*i.e.* Sommerfeld's condition) is easy to use but is not very accurate. Non-local non-reflective boundary conditions [11, 48] and BEM–FEM coupling [26] have been proposed, which give the perfect accuracy but yield expensive additional costs due to their non-local nature, leading to dense matrix blocks into the discrete weak formulation. As a good compromise between accuracy and computational cost, local high-order absorbing boundary conditions (HABCs) [3, 34, 51] and perfectly matched layers (PMLs) [8, 9, 75] provide high accuracy (at least for problems with homogeneous media) at the price of a larger number of unknowns and associated computational cost. The accuracy and the cost can be controlled by choosing the order of the HABC or the thickness of the PML. Usually, PMLs are easier to implement than HABCs, but the selection of the tuning parameters of a HABC is simpler to manage. In this article, we consider the HABC developed in [61].

Once the weak formulation is discretized thanks to the FEM with HABCs, the sparse linear system remains to be solved. It is well-known that this issue is still problematic since the sparse complex-valued linear system is very large and highly indefinite, most particularly for high frequencies. A direct solver cannot be used and standard Krylov iterative solvers are extremely difficult to make converge. A natural alternative solution which has been introduced more than 30 years ago is to use an iterative/direct hybrid approach based on a domain decomposition of the large global computational domain, and iterate between the subdomains where local subproblems are solved in parallel by a direct solver. Tremendous efforts have been made to develop efficient domain decomposition methods (DDMs) with good rate of convergence (see *e.g.* [30, 66, 74] for general introductions). For Helmholtz-type problems, we can mention Schwarz methods with overlap [17, 44, 53] or without overlap [6, 23, 40], FETI algorithms [27, 37–39] and the method of polarized traces [78], which are eventually combined with preconditioning techniques (see *e.g.* [25, 46, 49, 69, 70, 76]). A recent overview of these methods has been proposed by Gander and Zhang [45].

In this work, we investigate a domain decomposition approach with non-overlapping subdomains, which minimizes the data transfer between subdomains. It is admitted that the convergence rate of the non-overlapping DDMs strongly depends on the transmission condition enforced on the interfaces between the subdomains. The optimal transmission operator corresponds to the non-local Dirichlet-to-Neumann (DtN) map related to the complementary of the subdomain, which is a Schur complement at the discrete level. Since the cost of computing the exact DtN is prohibitive, strategies based on approximate DtN operators started to be investigated in the late 80's and early 90's (see *e.g.* [50, 62]). For Helmholtz-type problems, Després [6, 28] used Robin-type transmission conditions and proved that the iterative DDM converges. The Robin-type operator is a coarse approximation of the exact DtN operator which is sometimes used as a basic absorbing boundary condition (Sommerfeld's ABC). Improved Schwarz methods with optimized transmission conditions based on modified second-order transmission operators have next been introduced in [40, 65]. In parallel, FETI methods were adapted to Helmholtz problems as FETI-H [27, 37] and FETI-DPH [39] techniques, which can be interpreted as substructuring DDMs with optimized transmission conditions and preconditioning techniques. Later, domain decomposition strategies with HABC-based transmission conditions were developed to improve the convergence rate and robustness of the methods [13, 14, 52, 57], as well as PML-based approaches [4, 68, 69, 76] and non-local transmission conditions [24, 54, 71]. As for ABCs, transmission boundary conditions related to HABCs and PML represent a good compromise between the basic impedance conditions (which lead to suboptimal convergence) and the exact Dirichlet-to-Neumann (DtN) map related to the complementary of the subdomain (which is expensive to compute).

In the perspective of large-scale applications, the DDMs must be applicable with domain partitions having interior cross-points (where more than two subdomains meet) and boundary cross-points (that belong to both the exterior boundary and at least two subdomains). For non-overlapping DDMs, the cross-points require special care at both continuous and discrete levels. For Robin-type operators, the convergence is proved for the continuous case and mixed finite element discretizations in [6, 28]. These proofs are extended for more general abstract operators in [23]. Several approaches have been proposed

for nodal finite element discretizations. In the FETI framework, dual methods, of which [27, 37] are examples, lead to saddle point problems with constraints associated to the cross-points. These constraints can be redundant (see *e.g.* [30, 66, 74] for more details). The direct discretizations of the optimized Schwarz methods described in [40, 65] belong to this category. In the context of elliptic problems, several non-standard discretizations at the cross-points have been investigated in [41–43, 56]. With primal–dual methods, such as FETI-DPH [39] and the method proposed in [7, 12], global variables are associated to the physical fields at the cross-points. When combined with a preconditioning technique, this approach improves the convergence, but it requires all-to-all communications to solve a global system, which could deteriorate the parallel scaling of the method. Recently, cross-point treatments have been investigated for second-order transmission operators [29, 64] and non-local transmission approaches [21, 22]. PML-type operators have been tested in configurations with cross-points, but only in the context of DDM preconditioning [4, 55, 68]. The treatment of interior cross-points for optimized solvers with HABC-based, PML-based and non-local transmission conditions is a complicated problem which has, to the best of our knowledge, not been carefully addressed.

In the present paper and following [14], we consider an optimized non-overlapping DDM with a transmission condition based on a Padé-type HABC operator. In [14], no specific cross-point treatment was used on both interior and boundary cross-points. In addition, only first- and second-order exterior ABCs were considered. Here, we address the question of the cross-point treatment when the HABC operator is used in the transmission condition, or when it is used in the exterior boundary condition, or both. By contrast with the works reviewed in the previous paragraph, a specific care is required already at the continuous level. Indeed, for a complete definition of the local problems defined on the subdomains, additional conditions are required at the interior corners of the subdomains. Following the recent contribution [61] on the treatment of corners with HABCs, we introduce suited corner conditions into the variational formulation of the subproblems and additional transmission variables at the cross-points. The obtained cross-point treatment accelerates the convergence of the method with a very limited overcost. When a HABC is used as an exterior condition, the cross-point treatment is actually necessary, since the method cannot converge without it. While the approach is designed for regular lattice-type domain partition (*i.e.* with only parallel and perpendicular interfaces) and wave propagation in homogeneous media, it gives very good results with distorted partitions and smoothly varying heterogeneous media.

The paper is organized as follows. In Section 2, we present the Helmholtz boundary-value problem with a HABC and its suitable corner treatment based on adding suitable boundary conditions. The nodal FEM formulation is given next. Section 3 introduces the optimized Schwarz DDM with high-order transmission boundary conditions. The cross-point treatment is detailed for two subdomains and then for the multi-subdomain decomposition. The FEM formulation is next stated and some technical aspects about the algorithmic procedure are discussed. In Section 4, we propose some numerical examples to analyze the behavior of the proposed method. Three model configurations with lattice-type partitions are considered for the convergence study. The sensitivity of the method to the tuning parameters of the HABC operator is studied, as well as the influence of the frequency, the mesh refinement and the number of subdomains. After, a numerical investigation with heterogeneous media and distorted partitions is proposed. Finally, we conclude in Section 5.

2 Helmholtz problem with HABC and corner treatment

To describe the method, we consider a two-dimensional Helmholtz problem defined on a rectangular computational domain Ω,

$$\begin{cases} -\Delta u - \kappa^2 u = s, & \text{in } \Omega, \\ \partial_{n_f} u + \mathcal{B}_f u = 0, & \text{on each } \Gamma_f, \end{cases} \tag{1}$$

where κ is the wavenumber, assumed to be a positive constant, and $s(\mathbf{x})$ is a source term. In the numerical simulations, the source term is replaced with a scattering object. The edges of the rectangle are denoted by Γ_f ($f = 1 \dots 4$). For each edge Γ_f, ∂_{n_f} is the (exterior) normal derivative and $\mathcal{B}_f$ is an impedance operator which takes into account the behavior of waves outside the computational domain, that we suppose to be the free-space here. We take the convention that the time-dependence of the fields is $e^{-\imath\omega t}$, where ω is the angular frequency and t is the time.

To simulate wave propagation in free-space, the simplest boundary condition is the Sommerfeld Absorbing Boundary Condition (ABC), which corresponds to using the impedance operator $\mathcal{B}_f = -\imath\kappa$ on the edges. This condition is cheap and easy to use, but the accuracy is known to be poor. In this work, we consider Padé-type high-order absorbing boundary conditions (HABCs) [3, 34, 51, 61], which provide a better accuracy. To preserve the accuracy at the corners of the rectangle, a specific treatment based on compatibility relations derived in [61] is used leading to very low spurious reflections at the boundary. For the HABC, a finite element implementation of the problem is described later. Let us remark that other alternative solutions could be considered for truncating the free-space, like for example by using the well-known Perfectly Matched Layer (PML) approach introduced by Bérenger in [8] and studied *e.g.* in [9, 75] for Helmholtz-type problems. Nevertheless, we do not address this situation here since PMLs are related to the introduction of a surrounding layer which is out of the framework presented here.

2.1 High-order absorbing boundary condition (HABC)

The Padé-type HABC is obtained by approximating an exact non-reflecting boundary condition derived for planar boundaries. Assuming that the exterior medium is homogeneous and free of sources, solving the exterior half-space problem gives the exact (non-local) boundary condition $\partial_n u + \mathcal{B}^{\text{ex}} u = 0$, with the (pseudo-differential) impedance operator $\mathcal{B}^{\text{ex}}$ defined as

$$\mathcal{B}^{\text{ex}} = -\imath\kappa\sqrt{1+\partial_{\tau\tau}/\kappa^2}, \tag{2}$$

where ∂_n and ∂_τ are respectively the (exterior) normal and tangential derivatives (see *e.g.* [34]). Following [59], this operator is localized by using a Padé approximation of the square-root after a rotation of the branch-cut. For each face Γ_f, this leads to the HABC impedance operator

$$\mathcal{B}_f = -\imath\kappa\alpha_f\left[1+\frac{2}{M_f}\sum_{i=1}^{N_f} c_{f,i}\left(1-\alpha_f^2(c_{f,i}+1)\left[(\alpha_f^2 c_{f,i}+1)+\partial_{\tau_f\tau_f}/\kappa^2\right]^{-1}\right)\right], \tag{3}$$

with $\alpha_f = e^{\imath\phi_f/2}$, $c_{f,i} = \tan^2(i\pi/M_f)$ and $M_f = 2N_f+1$. The accuracy of the Padé-type HABC depends on the number of terms N_f and the angle of rotation ϕ_f (see [51, 61] for further details). In particular, the parameters $N_f = 0$ and $\phi_f = 0$ yield $\mathcal{B}_f = -\imath\kappa$, which corresponds to the basic ABC.

For the effective implementation of the HABC, N_f auxiliary fields $\{\varphi_{f,i}\}_{i=1\dots N_f}$ are defined on Γ_f, and the boundary condition is rewritten as

$$\partial_{n_f} u + B_f\Big(u, \{\varphi_{f,i}\}_{i=1\dots N_f}\Big) = 0, \quad \text{on } \Gamma_f, \tag{4}$$

with the operator B_f defined as

$$B_f\Big(u, \{\varphi_{f,i}\}_{i=1\dots N_f}\Big) = -i\kappa\alpha_f\left[u+\frac{2}{M_f}\sum_{i=1}^{N_f} c_{f,i}\,(u+\varphi_{f,i})\right]. \tag{5}$$

The additional fields are governed by the auxiliary equations

$$-\partial_{\tau_f\tau_f}\varphi_{f,i} - \kappa^2\left[(\alpha_f^2 c_{f,i}+1)\varphi_{f,i} + \alpha_f^2(c_{f,i}+1)u\right] = 0, \quad \text{on } \Gamma_f. \quad (i=1\dots N_f) \tag{6}$$

The linear multivariate function B_f is introduced to simplify the expressions in the remainder of the paper.

2.2 Corner treatment

When the HABC is prescribed on a boundary with corners, a specific treatment must be used at the corners. Because of the second-order spatial derivative in equation (6), boundary conditions must be added on the auxiliary fields at the extremities of each edge, which are at the corners of the domain. In a previous work [61], we have analyzed several strategies to preserve the accuracy of the solution at

the corners. For configurations with right angles, the best approach consists in using a different set of auxiliary fields for each edge, with compatibility relations to couple the auxiliary fields of adjacent edges at the common corner.

Consider two adjacent edges Γ_f and $\Gamma_{f'}$ meeting at the corner $P_{f,f'} = \Gamma_f \cap \Gamma_{f'}$. Two sets of surface fields $\{\varphi_{f,i}\}_{i=1\dots N_f}$ and $\{\varphi_{f',i'}\}_{i'=1\dots N_{f'}}$ are defined on Γ_f and $\Gamma_{f'}$, respectively. Globally, a total of $N_f + N_{f'}$ boundary conditions must be written on these auxiliary fields at the corner $P_{f,f'}$. Following the approach detailed in [61], well-suited conditions are such that

$$\partial_{n_{f'}}\varphi_{f,i} + B_{f'}\Big(\varphi_{f,i}, \{\psi_{ff',ii'}\}_{i'=1\dots N_{f'}}\Big) = 0, \quad \text{on } P_{ff'}, \quad (i = 1\dots N_f) \tag{7}$$

$$\partial_{n_f}\varphi_{f',i'} + B_f\Big(\varphi_{f',i'}, \{\psi_{f'f,i'i}\}_{i=1\dots N_f}\Big) = 0, \quad \text{on } P_{ff'}, \quad (i' = 1\dots N_{f'}) \tag{8}$$

with $N_f \times N_{f'}$ auxiliary variables $\{\psi_{ff',ii'}\}_{i=1\dots N_f, i'=1\dots N_{f'}}$ defined as

$$\psi_{ff',ii'} = -\frac{\alpha_{f'}^2(c_{f',i'}+1)\varphi_{f,i} + \alpha_f^2(c_{f,i}+1)\varphi_{f',i'}}{\alpha_f^2 c_{f,i} + \alpha_{f'}^2 c_{f',i'} + 1}, \quad \text{on } P_{ff'}. \quad (i = 1\dots N_f, i' = 1\dots N_{f'}) \tag{9}$$

Let us remark that $\psi_{f'f,i'i} = \psi_{ff',ii'}$. In a nutshell, the HABC defined on the field u on one edge is also imposed on the auxiliary fields living on the adjacent edge at the common corner [61], with new auxiliary variables defined at the corner. For instance, the HABC set on $\Gamma_{f'}$ is also forced on the fields $\{\varphi_{f,i}\}_{i=1\dots N_f}$ at $P_{f,f'}$ (equation (7)).

As a particular case, let us consider a configuration with a HABC given on Γ_f and the basic ABC set on the adjacent edge $\Gamma_{f'}$, *i.e.*

$$\partial_{n_f} u + B_f\Big(u, \{\varphi_{f,i}\}_{i=1\dots N_f}\Big) = 0, \quad \text{on } \Gamma_f, \tag{10}$$

$$\partial_{n_{f'}} u - \imath\kappa u = 0, \quad \text{on } \Gamma_{f'}. \tag{11}$$

At the corner $P_{f,f'}$, N_f boundary conditions must be imposed on the auxiliary fields living on Γ_f. Following the approach, the basic ABC must be prescribed

$$\partial_{n_{f'}}\varphi_{f,i} - \imath\kappa\varphi_{f,i} = 0, \quad \text{on } P_{f,f'}, \quad (i = 1\dots N_f) \tag{12}$$

which corresponds to equation (7) with $N_{f'} = 0$ and $\phi_{f'} = 0$.

2.3 Finite element formulation

The problem finally consists in solving the main field u on the rectangular domain with a HABC on each edge by (4). Auxiliary fields defined on the edges are governed by 1D Helmholtz equations through (6) and are coupled at the corners by auxiliary relations by (7)-(8) and auxiliary variables using (9). If the basic ABC is given for the main field on an edge, there is no auxiliary field on that edge, and the basic ABC is prescribed on the auxiliary variables living on the adjacent edges at the common corners.

In order to solve the problem with a finite element scheme, we straightforwardly adapt the bilinear form of the Helmholtz equation. The variational formulation of the problem reads: find $u \in H^1(\Omega)$ and $\varphi_{f,i} \in H^1(\Gamma_f)$, for $f = 1\dots 4$ and $i = 1\dots N_f$, such that

$$\int_\Omega \Big[\nabla u\cdot\nabla v - \kappa^2 uv\Big]\,d\Omega + \sum_{f=1}^{4}\int_{\Gamma_f} B_f\big(u, \{\varphi_{f,i}\}_{i=1\dots N_f}\big)v\,d\Gamma = \int_\Omega sv\,d\Omega, \quad \forall v \in H^1(\Omega),$$

and

$$\int_{\Gamma_f}\Big[\big(\partial_{\tau_f}\varphi_{f,i}\big)\big(\partial_{\tau_f}\rho_f\big) - \kappa^2\big((\alpha_f^2 c_{f,i}+1)\varphi_{f,i} + \alpha_f^2(c_{f,i}+1)u\big)\rho_f\Big]\,d\Gamma$$
$$+ \sum_{f'}\Big[B_{f'}\big(\varphi_{f,i}, \{\psi_{ff',ii'}\}_{i'=1\dots N_{f'}}\big)\rho_f\Big]_{P_{ff'}} = 0, \quad \forall \rho_f \in H^1(\Gamma_f).$$

In the last equation, the index f' corresponds to any edge $\Gamma_{f'}$ adjacent to Γ_f, and the variables $\{\psi_{ff',ii'}\}_{i'=1\dots N_{f'}}$ are defined on $P_{ff'}$ by equation (9). Standard Lagrange finite elements can then be used to discretize the problem.

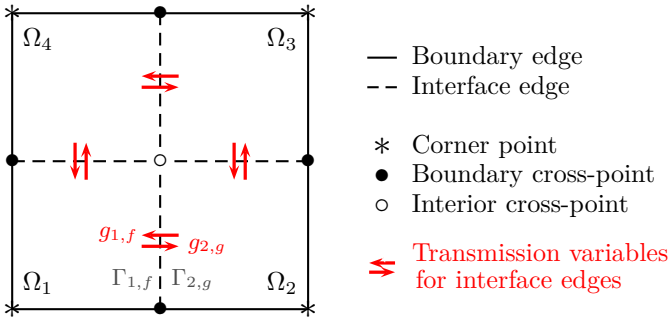

Figure 1: Terminology and transmission variables across the interface edges. In this example, the continuity of the local solution u_1 and u_2 on the interface edge $\Gamma_{1,f} = \Gamma_{2,g}$ is ensured thanks to the transmission variables $g_{1,f}$ and $g_{2,g}$.

3 Domain decomposition method with cross-point treatment

In this section, we present a non-overlapping domain decomposition method (DDM) for lattice-type partitions of the domain. The convergence of the method is accelerated by using a Padé-type HABC as a transmission condition with a novel strategy to deal with cross-points. This strategy relies on the corner treatment derived for the HABCs in the previous section. The DDM and the cross-point strategy are presented in Sections 3.1 and 3.2, respectively. The finite element scheme and the algorithmic procedure are described in Section 3.3.

We consider a partition of the rectangular domain Ω into a grid of rectangular non-overlapping subdomains Ω_I ($I = 1 \dots N^{\text{dom}}$). The edges of each subdomain Ω_I are denoted by $\Gamma_{I,f}$ ($f = 1 \dots 4$). Each edge is either a *boundary edge* if it belongs to the boundary of the global domain ($\Gamma_{I,f} \subset \partial\Omega$), or an *interface edge* if there is a neighboring subdomain beyond the edge ($\Gamma_{I,f} \not\subset \partial\Omega$). In this decomposition, two kinds of points deserve attention: the *boundary cross-points* that belong to two subdomains and that touch the boundary of the global domain, and the *interior cross-points* belonging to four subdomains and that do not touch the boundary of the global domain. These edges and points are illustrated in Figure 1 for a 2×2 partition.

3.1 Optimized Schwarz-type domain decomposition method (DDM)

Following the standard optimized Schwarz-type method, the global problem (1) is decomposed into local subproblems defined on the subdomains. The solution u_I for the subdomain Ω_I is obtained by solving

$$\begin{cases} -\Delta u_I - \kappa^2 u_I = s, & \text{in } \Omega_I, \\ \partial_{n_{I,f}} u_I + \mathcal{B}_{I,f} u_I = g_{I,f}, & \text{on each } \Gamma_{I,f}, \end{cases} \tag{13}$$

where $\mathcal{B}_{I,f}$ is an impedance operator and $g_{I,f}$ is a transmission variable which is set to zero if $\Gamma_{I,f}$ is a boundary edge, while it depends on the local solution belonging to the neighboring subdomain if $\Gamma_{I,f}$ is an interface edge. In the latter case, to ensure the compatibility with the global problem, the transmission variable is defined as

$$g_{I,f} = \partial_{n_{I,f}} u_J + \mathcal{B}_{I,f} u_J, \tag{14}$$

where u_J is the solution of the neighboring subdomain Ω_J. Since a subproblem similar to system (13) is defined on Ω_J, another transmission condition is prescribed on the edge shared by Ω_I and Ω_J. Denoting the shared interface edge as $\Gamma_{J,g} = \Gamma_{I,f}$, the transmission condition reads

$$\partial_{n_{J,g}} u_J + \mathcal{B}_{J,g} u_J = g_{J,g} \tag{15}$$

with a supplementary transmission variable defined as $g_{J,g} = \partial_{n_{J,g}} u_I + \mathcal{B}_{J,g} u_I$. If we assume that the impedance operators used on both sides of the interface are the same, which means $\mathcal{B}_{I,f} = \mathcal{B}_{J,g}$, we have

$$g_{I,f} = -g_{J,g} + 2\mathcal{B}_{J,g} u_J, \tag{16}$$

by combining equations (14) and (15).

In the global iterative DDM procedure, each iteration consists in solving concurrently all the subproblems (13) and updating the transmission variables using equation (16) (see Section 3.3 for further details). For a fast convergence of this procedure, the impedance operators used at the interface edges must be chosen wisely. Ideally, for a given subdomain, the operators should correspond to the DtN map related to the complementary of the subdomain. Approximations of this DtN map are also used to define ABCs. Indeed, if there is no source outside the subdomain, the transmission variables in the local system (13) are canceled, and the transmission conditions should be non-reflecting boundary conditions.

Following [14], the impedance operators for the transmission conditions are based on Padé-type HABCs. For each subdomain Ω_I, the local solution u_I verifies

$$\begin{cases} -\Delta u_I - \kappa^2 u_I = s, & \text{in } \Omega_I, \\ \partial_{n_{I,f}} u_I + B_{I,f}\Big(u_I, \{\varphi_{I,f,i}\}_{i=1\dots N_{I,f}}\Big) = g_{I,f}, & \text{on each } \Gamma_{I,f}, \end{cases} \tag{17}$$

with the transmission variable $g_{I,f}$ that verifies

$$g_{I,f} = \begin{cases} 0, & \text{if } \Gamma_{I,f} \subset \partial\Omega, \\ -g_{J,g} + 2B_{J,g}\Big(u_J, \{\varphi_{J,g,j}\}_{j=1\dots N_{J,g}}\Big), & \text{if } \Gamma_{I,f} \not\subset \partial\Omega. \end{cases} \tag{18}$$

The second equation of system (17) is a boundary condition if $\Gamma_{I,f}$ is a boundary edge, or a transmission condition if $\Gamma_{I,f}$ is an interface edge. In both cases, if $N_{I,f} > 0$, auxiliary fields $\{\varphi_{I,f,i}\}_{i=1\dots N_{I,f}}$ are defined on the edge, and are governed by

$$-\partial_{\tau_{I,f}\tau_{I,f}}\varphi_{I,f,i} - \kappa^2\left[(\alpha_{I,f}^2 c_{I,f,i} + 1)\varphi_{I,f,i} + \alpha_{I,f}^2(c_{I,f,i}+1)u_I\right] = 0, \quad \text{on } \Gamma_{I,f}, \tag{19}$$

with $i = 1 \dots N_{I,f}$. The parameters of the transmission conditions used on both sides of an interface edge must be the same (*i.e.* $N_{I,f} = N_{J,g}$ and $\phi_{I,f} = \phi_{J,g}$, with $\Gamma_{I,f} = \Gamma_{J,g}$), since we assumed that the impedance operators are the same on a shared interface. For consistency, the same boundary condition must be prescribed on the boundary edges of the subdomains and on the corresponding edges of the global domain.

Boundary conditions must be set on the auxiliary fields at the extremities of the edges because of the second-order partial derivative in the governing equation (19). The extremities of an edge are at corners of a subdomain, and correspond to interior cross-points, boundary cross-points or corners of the global domain. The cross-point treatment, described in the next section, actually provides the missing boundary conditions at the cross-points.

3.2 Dealing with cross-points

The cross-point treatment relies on the corner treatment described in Section 2. It is applied at the corners of the subdomains. Depending on the configuration, it provides boundary conditions or transmission conditions for the auxiliary fields at the cross-points. In the latter case, new transmission variables are defined at the cross-points.

3.2.1 Two-subdomain case

To describe the approach, we first consider a partition of the rectangular domain Ω into two rectangular subdomains with an interface Γ and two boundary cross-points. Three configurations, represented on Figure 2, are studied: the basic ABC prescribed on $\partial\Omega$ with a HABC-based transmission condition on Γ (Configuration 1), a HABC on $\partial\Omega$ with a transmission condition based on the basic ABC on Γ (Configuration 2), and the HABC operator used both for $\partial\Omega$ and Γ (Configuration 3). Because the HABC is used on the exterior boundary and/or the interface, a specific treatment must be used at the boundary cross-points.

In the first configuration (Figure 2a), auxiliary fields are defined on both sides of the interface. These fields require boundary conditions at the extremities of the interface, which are corners of the subdomains.

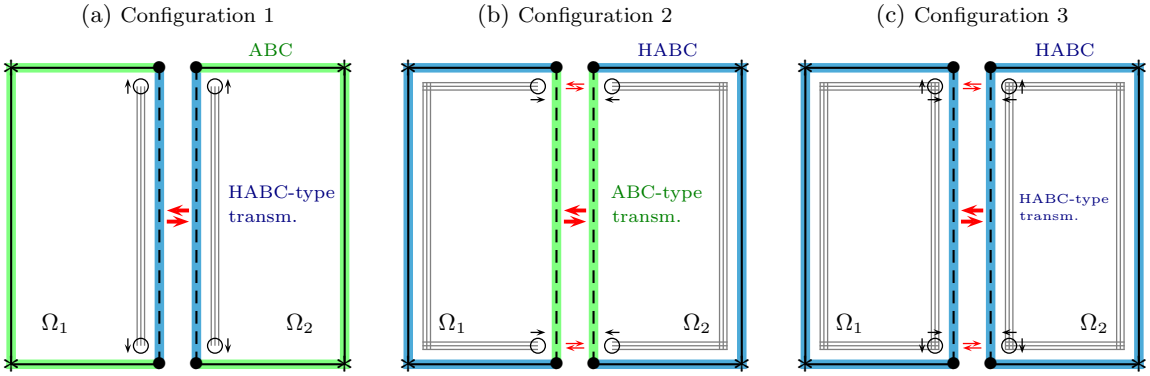

Figure 2: Three configurations for two-subdomain case. The exterior boundary condition is a basic ABC or a HABC, and the transmission condition is based on the HABC operator or the basic ABC operator. The thin gray lines illustrate the position of auxiliary fields. The black arrows indicate where boundary conditions are required for auxiliary fields. The red arrows indicate transmission conditions on the edge or at the cross-points.

The basic ABC is set on the adjacent edges (*i.e.* the upper and lower boundary edges). Following the strategy of Section 2, the basic ABC is also given on the auxiliary fields at the boundary cross-points.

In the second configuration (Figure 2b), a HABC is given on each global edge Γ_f in the global problem, auxiliary fields are defined on each edge and the corner treatment is used. After the domain partition, a HABC is imposed on each boundary edge $\Gamma_{I,f}$ of each subdomain Ω_I, and a set of auxiliary fields is defined on each of these edges. For the consistency of the global problem, the parameters of the HABC on $\Gamma_{I,f}$ must be the same as the parameters of the HABC given on the global edge $\Gamma_f \supset \Gamma_{I,f}$. For a global edge Γ_f that has been divided by the partitioning (upper and lower edges in Figure 2b), the continuity of the auxiliary fields must be enforced at the cross-points. As the ABC-based transmission condition is used on the main field on the interface, this transmission condition is also used on each auxiliary field at the boundary cross-points and auxiliary transmission variables are defined at these points.

The last configuration combines the difficulties. The exterior boundary condition and the transmission condition are based on HABCs (Figure 2c). The auxiliary fields living on every edge require boundary conditions at the boundary cross-points. To deal with this case, we recall that the operators used on the edges of each subdomain should approximate the DtN map of the free-space if the exterior medium relative to each subdomain is homogeneous. If the transmission variables are canceled, it corresponds to forcing a HABC on every edge. Therefore, we apply the corner treatment described in Section 2 to all the corners of the subdomains, which gives boundary conditions for the auxiliary fields. If the transmission variables are not canceled, the continuity of the fields $\{u_I\}_{I=1,2}$ is enforced at the interface thanks to the right-hand side of the second equation of system (13). For the auxiliary fields living on the boundary edges, the boundary conditions at the cross-point become transmission conditions by adding transmission variables in the right-hand sides, as for the second configuration. These transmission variables verify relations similar to equation (18) at the cross-points.

3.2.2 Multi-subdomains case

In the general case, the rectangular domain Ω is partitioned into a grid of rectangular subdomains, with interior and boundary cross-points. The strategy relies on the following principles, which generalize the approaches used for the three previous configurations:

- The same transmission condition is used on both sides of each interface edge. The boundary condition used on each boundary edge is the same as the one prescribed on the corresponding edge of the global domain. In the domain partition, the HABC operators used on edges that are on a same line have the same parameters (*e.g.* in Figure 3: the top edges of Ω_1 and Ω_2, the top edges of Ω_3 and Ω_4, the left edges of Ω_1 and Ω_4, ...).
- If auxiliary fields are defined on an edge $\Gamma_{I,f}$ of a subdomain Ω_I, boundary conditions or trans-

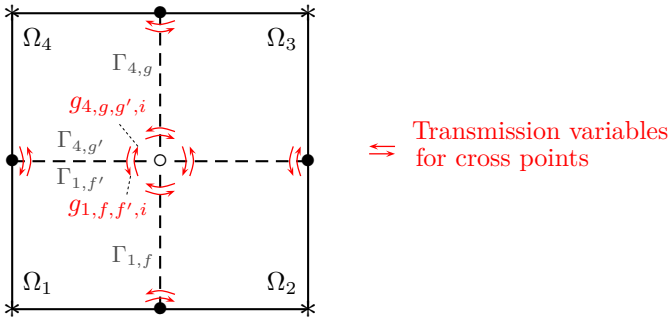

Figure 3: Transmission variables across the boundary and interior cross-points, if the HABC operator is used both in the exterior boundary condition and in the interface conditions. In the example, the continuity of the auxiliary fields $\varphi_{1,f,i}$ and $\varphi_{4,g,i}$ (defined on the aligned edges $\Gamma_{1,f}$ and $\Gamma_{4,g}$) at the interior cross-point $P_{1,ff'} = P_{4,gg'}$ is ensured thanks to the transmission variables $g_{1,ff',i}$ and $g_{4,gg',i}$. These variables verify equation (21).

mission conditions must be set on these fields at the extremities of this edge (which can be interior cross-points, boundary cross-points, or corners of Ω). These conditions are given by the condition already used for u_I on the adjacent edges. If a transmission condition is used on u_I on an adjacent edge, transmission conditions are considered on the auxiliary fields at the cross-point, and new transmission variables are introduced.

- The corner treatment described in Section 2 is used at the corners of each subdomain, which gives boundary conditions to the auxiliary fields living on the edges. At the cross-points, these conditions can become transmission conditions by adding transmission variables in the right-hand sides, which are similar to equation (18).

Following these principles, the description of the problem with domain decomposition can be completed.

For each subdomain Ω_I, the local solution u_I verifies equations (17). For each edge $\Gamma_{I,f}$, the transmission variable $g_{I,f}$ satisfies equation (18). Each auxiliary field $\varphi_{I,f,i}$ $(i = 1 \dots N_{I,f})$ defined on a boundary or interface edge $\Gamma_{I,f}$ is such that

$$\begin{cases} -\partial_{\tau_{I,f}\tau_{I,f}}\varphi_{I,f,i} - \kappa^2\big((\alpha_{I,f}^2 c_{I,f,i}+1)\varphi_{I,f,i} + \alpha_{I,f}^2(c_{I,f,i}+1)u_I\big) = 0, & \text{on } \Gamma_{I,f}, \\ \partial_{n_{I,f'}}\varphi_{I,f,i} + B_{I,f'}\left(\varphi_{I,f,i}, \{\psi_{I,ff',ii'}\}_{i'=1\dots N_{I,f'}}\right) = g_{I,ff',i}, & \text{on each } P_{I,ff'}, \end{cases} \tag{20}$$

with the transmission variable $g_{I,ff',i}$

$$g_{I,ff',i} = \begin{cases} 0, & \text{if } \Gamma_{I,f'} \subset \partial\Omega, \\ -g_{J,gg',i} + 2B_{J,g}\left(\varphi_{J,g,i}, \{\psi_{J,gg',ii'}\}_{i'=1\dots N_{J,g'}}\right), & \text{if } \Gamma_{I,f'} \not\subset \partial\Omega. \end{cases} \tag{21}$$

In these relations, $\Gamma_{I,f'}$ is any edge that is adjacent to $\Gamma_{I,f}$, and $P_{I,ff'} = \Gamma_{I,f} \cap \Gamma_{I,f'}$ is the corner that is shared by these edges. The second equation of system (20) is a boundary condition if $\Gamma_{I,f'}$ is a boundary edge, or a transmission condition if $\Gamma_{I,f'}$ is an interface edge. The transmission variable is set to zero in the former case, and it depends on the solution of the other side of $\Gamma_{I,f'}$ in the latter case. The variables $\psi_{I,ff',ii'}$ are defined using equation (9).

In equation (21), the indices are chosen in such a way that Ω_J is the neighboring subdomain on the other side of $\Gamma_{I,f'}$, the edge $\Gamma_{J,g'}$ is shared by the subdomains (*i.e.* $\Gamma_{I,f'} = \Gamma_{J,g'}$), and the edge $\Gamma_{J,g}$ is aligned with $\Gamma_{I,f}$ (*i.e.* $f = g$), as illustrated in Figure 3. The variable $g_{J,gg',i}$ is used in a transmission condition for an auxiliary field $\varphi_{J,g,i}$ living on $\Gamma_{J,g}$. Therefore, the transmission conditions enforce the continuity of the auxiliary fields $\varphi_{I,f,i}$ and $\varphi_{J,g,i}$, which live on edges that are on the same line. Let us note that, since the HABC parameters are the same for edges that are aligned, $N_{I,f} = N_{J,g}$ and $\phi_{I,f} = \phi_{J,g}$.

3.3 Finite element scheme and algorithmic procedure

Each step of the DDM iterative procedure consists in solving a local subproblem on each subdomain, and updating the transmission variables both on the interface edges and at the cross-points. The numerical solution of the subproblems is performed with a standard nodal finite element scheme built on a conformal mesh made of triangles or quadrangles. For each subdomain Ω_I, the variational formulation of the subproblem reads: find $u_I \in H^1(\Omega_I)$ and $\varphi_{I,f,i} \in H^1(\Gamma_{I,f})$, with $i = 1 \dots N_{I,f}$ and $f = 1 \dots 4$, such that

$$\int_{\Omega_I} \Big[\nabla u_I \cdot \nabla v_I - \kappa^2 u_I v_I\Big]\, d\Omega_I + \sum_{f=1}^{4} \int_{\Gamma_{I,f}} B_{I,f}\Big(u_I, \{\varphi_{I,f,i}\}_{i=1\dots N_{I,f}}\Big) v_I \, d\Gamma_{I,f}$$
$$= \int_{\Omega_I} s v_I \, d\Omega_I + \sum_{f=1}^{4} \int_{\Gamma_{I,f}} g_{I,f} v_I \, d\Gamma_{I,f}, \qquad \forall v_I \in H^1(\Omega_I), \quad (22)$$

and

$$\int_{\Gamma_{I,f}} \Big[(\partial_{\tau_{I,f}} \varphi_{I,f,i})\,(\partial_{\tau_{I,f}} \rho_{I,f}) - \kappa^2 \Big((\alpha_{I,f}^2 c_{I,f,i} + 1)\varphi_{I,f,i} + \alpha_{I,f}^2 (c_{I,f,i} + 1) u_I\Big)\, \rho_{I,f}\Big]\, d\Gamma_{I,f}$$
$$+ \sum_{f'} \Big[B_{I,f'}\Big(\varphi_{I,f,i}, \{\psi_{I,ff',ii'}\}_{i'=1\dots N_{I,f'}}\Big)\, \rho_{I,f}\Big]_{P_{I,ff'}}$$
$$= \sum_{f'} \Big[g_{I,ff',i}\, \rho_{I,f}\Big]_{P_{I,ff'}}, \qquad \forall \rho_{I,f} \in H^1(\Gamma_{I,f}). \quad (23)$$

In the last equation, the index f' corresponds to any edge $\Gamma_{I,f'}$ adjacent to $\Gamma_{I,f}$, and $P_{I,ff'} = \Gamma_{I,f} \cap \Gamma_{I,f'}$ is the shared corner. The variables $\psi_{I,ff',ii'}$ are defined using (9). This variational formulation is an extension of the one used in [14] (see equation (62) in that reference). In that work, there is only one set of auxiliary fields and equations on the subdomain boundary $\partial\Omega_I$. Here, there is one set for each edge $\Gamma_{I,f}$ of the subdomain, and new terms appear in (23) to deal with the corners of the subdomain.

In the DDM iterative procedure, the transmission variables computed at an iteration n are used in the right-hand side of equations (22)-(23) to compute the local fields of the iteration $n+1$. The transmission variables are then updated using equations (18)-(21). Therefore, at each iteration, the *interface* transmission variables are computed using

$$g_{I,f}^{(n+1)} = -g_{J,g}^{(n)} + 2B_{J,g}\Big(u_J^{(n+1)}, \{\varphi_{J,g,j}^{(n+1)}\}_{j=1\dots N_{J,g}}\Big), \quad (24)$$

for each interface edge $\Gamma_{I,f} \not\subset \partial\Omega$. Similarly, the *cross-point* transmission variables are updated through

$$g_{I,ff',i}^{(n+1)} = -g_{J,gg',i}^{(n)} + 2B_{J,g}\left(\varphi_{J,g,i}^{(n+1)}, \{\psi_{J,gg',ii'}^{(n+1)}\}_{i'=1\dots N_{J,g'}}\right), \quad (25)$$

at each cross-point $P_{I,ff'}$, with $\Gamma_{I,f'} \not\subset \partial\Omega$.

The global process can be recast as one application of an iterative operator $\mathcal{A} : \mathcal{G} \to \mathcal{G}$ defined by

$$g^{(n+1)} = \mathcal{A} g^{(n)} + b, \quad (26)$$

where $g^{(n)} \subset \mathcal{G}$ is the set of transmission data, and b depends on the source term s. This can be seen as one iteration of the Jacobi method to solve the linear system $(\mathcal{I} - \mathcal{A})g = b$, where $\mathcal{I}$ is the identity operator. Following a well-known strategy (see *e.g.* [7, 14]), a GMRES Krylov subspace iterative solver is used on the top of the DDM procedure to solve this linear system efficiently. Here, by contrast with most of the works, the transmission data contains transmission variables associated to both interfaces and cross-points.

4 Numerical results

This section reports some finite element simulations to study the HABC-based domain decomposition method with cross-point treatment. After a description of three benchmarks in Section 4.1, we analyze the

(a) Configuration 1 (b) Configuration 2 (c) Configuration 3

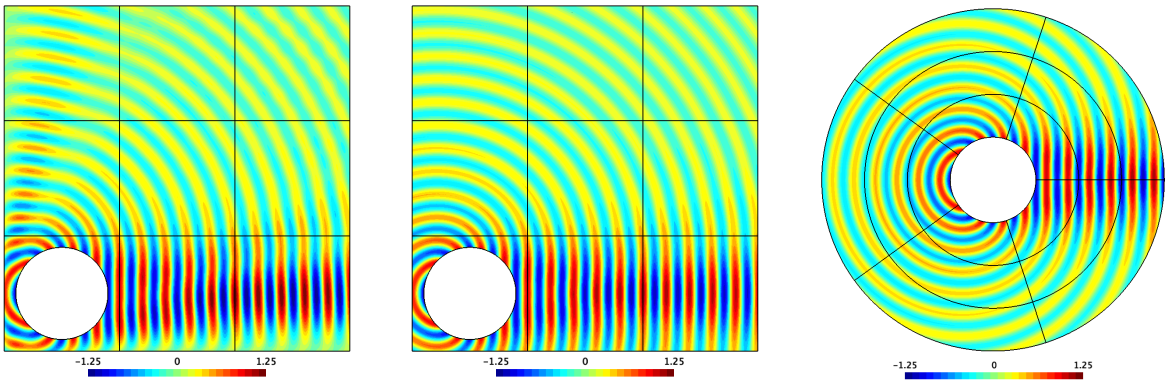

Figure 4: Scattering benchmarks: real part of the scattered field of the reference numerical solution for the three configurations with $\kappa = 4\pi$. The basic ABC, a HABC and the second-order Bayliss–Turkel ABC are set on the exterior border, respectively.

convergence history (Section 4.2), the sensitivity to the HABC parameters (Section 4.3) and the influence of the wavenumber, the mesh density and the number of subdomains on the convergence rate (Section 4.4). Finally, configurations with distorted domains partitions and smoothly varying heterogeneous media are investigated in Section 4.5.

4.1 Description of the benchmarks

The reference benchmark used through this section is the scattering of an incident plane wave $u^{\text{inc}}(\mathbf{x}) = e^{\imath\kappa x}$ by a sound-soft circular scatterer. For a circle of radius R centered at the origin, the scattered field is given by

$$u^{\text{ref}}(r,\theta) = -\sum_{m=0}^{\infty} \epsilon_m \imath^m \frac{J_m(\kappa R)}{H_m^{(1)}(\kappa R)} H_m^{(1)}(\kappa r)\cos(m\theta), \quad r \geq R, \tag{27}$$

where (r,θ) are the polar coordinates, J_m is the m^{th}-order Bessel's function, $H_m^{(1)}$ is the m^{th}-order first-kind Hankel function, and ϵ_m is the Neumann function which is equal to 1 for $m = 0$ and 2 otherwise.

Three configurations are considered. For the first configuration (Figure 4a), the finite element simulations are performed on the square computational domain $[-1.25, 6.25] \times [-1.25, 6.25]$ with checkerboard partitions. The scatterer is the unit disk centered at the origin. The basic ABC, *i.e.* $\partial_n u - \imath\kappa u = 0$, is set on the exterior boundary of the domain. Because this boundary condition is a rather inaccurate non-reflecting boundary treatment, the numerical solution contains both the scattered field and spurious waves reflected on the exterior boundary. For the second configuration (Figure 4b), the HABC is used on the edges of the square domain with the suited treatment at the corners. The HABC parameters $N = 6$ and $\phi = 0.3\pi$ have been selected to avoid any visible modeling error in the numerical solution (*i.e.* the numerical error due to the finite element scheme is significantly larger than the modeling error due to the approximate boundary condition — see [61]). For the third configuration (Figure 4c), we have considered a circular domain of radius $R_1 = 4$ with radial/longitudinal partitions. The second-order Bayliss–Turkel ABC [2, 5]

$$\partial_r u - \imath\kappa u + \frac{1}{2R_1} u - \frac{1}{8R_1^2(R_1^{-1} - \imath\kappa)} u - \frac{1}{2(R_1^{-1} - \imath\kappa)} \partial_{\tau\tau} u = 0, \tag{28}$$

is given on the exterior circular boundary, where $\partial_\tau = R_1^{-1}\partial_\theta$ is the tangential derivative over the circle of radius R_1 in polar coordinates (r,θ).

For all the configurations, the finite element scheme is based on meshes made of second-order curvilinear triangular elements and quadratic polynomial basis functions (P2). The Dirichlet BC $u = -u^{\text{inc}}$

is set at the boundary of the (sound-soft) scatterer. By default, the wavenumber is $\kappa = 4\pi$ and the characteristic number of vertices per wave length is $n_\lambda = 10$. The meshes of the square domain and the circular domain are made of 56 538 and 49 718 triangles, respectively. For the three configurations, the relative L^2-errors of the finite element solutions compared to the reference solution (27) are 2.2×10^{-1}, 2.4×10^{-3} and 1.7×10^{-3}, respectively. We used the GetDDM framework [73] which combines the mesh generator Gmsh [47] and the finite element solver GetDP [31].

4.2 Convergence analysis

We begin by analyzing the convergence of the DDM procedure with cross-point treatment for the different configurations. The relative L^2-errors and the relative residuals are plotted as functions of the number of the GMRES iterations in Figure 5 for the three configurations. The L^2-error is calculated by comparing the solution obtained in each subdomain to the reference numerical solution computed on the same mesh without domain decomposition. In every case, HABC-based transmission conditions with different numbers of auxiliary fields are tested ($N = 0$, 2, 4 and 6 with $\phi = 0.3\pi$). The effect of the cross-point treatment is analyzed by keeping or removing the corresponding terms in the finite element scheme. The latter case consists in setting a homogeneous Neumann BC on the auxiliary fields at the cross-points. On all the figures, the dotted lines are associated to results without the cross-point treatment.

For the first configuration (*i.e.* square domain with basic ABC), the relative residual and the relative error have the same order of magnitude in all the cases (Figures 5a-5b) and decrease during the iterations. Using the cross-point treatment clearly accelerates the convergence, especially for transmission conditions with large values of N. The number of iterations to reach a relative error of magnitude 10^{-6} is reduced by 20% to 40% thanks to the treatment. When the cross-point treatment is enabled, the decay of residual and error can be accelerated further, up to a certain point, by taking a number of auxiliary fields N sufficiently large. Taking higher values for N does not change the results, while, without the cross-point treatment, increasing N slightly slows down the decays.

The good results obtained with the cross-point treatment and N sufficiently large can be interpreted by looking at the numerical solution after each iteration (Figure 6). At the initialization, the right-hand side term of the iteration system is computed by solving each subproblem with source terms only (see Section 3). Here, only the subdomain containing the scattering disk has a source, and then non-zero solution (Figure 6a). The numerical solution in this subdomain is already rather accurate since the transmission condition acts as a HABC, and the cross-point treatment behaves as the suited corner treatment. Since there is neither source nor very significant reflected waves generated outside the subdomain, the HABC and the corner treatment constitute a very good boundary treatment for the subdomain. During the iterations, the signal is propagated from subdomain to subdomain. At the fourth iteration, the signal reaches the last subdomain. This coincides with a sharp reduction of both the residual and error by an order one in magnitude.

For the second configuration (*i.e.* square domain with HABC), the impact of the cross-point treatment is more important. When the cross-point treatment is not enabled, the residuals decrease with the iterations (Figure 5c), but the relative errors reach a plateau and stagnate at 10^{-1} (Figure 5d). This can be explained by noting the only difference with the previous configuration: a HABC is prescribed on the exterior boundary instead of a basic ABC, and auxiliary fields defined on the edges of the domain Ω. Without the cross-point treatment, the derivative of these auxiliary fields is set to zero at the boundary cross-points. Then, the problem with domain decomposition is not compatible with the original problem, and the iterative schemes converge towards a wrong solution. To fix this, the continuity of the auxiliary fields living on the boundary edges must be enforced at the boundary cross-points. With the cross-point treatment, transmission conditions are set at the boundary cross-points, and the error decays together with the residual, as it should be. It is worth to note that the absence of cross-point treatment in the first configuration does not break the convergence of the error because no auxiliary fields are defined on the boundary edges. In that case, the problem with domain partition is compatible with the original problem.

When comparing the results of the two first configurations for high values of N, we observe that the error decays faster for the second configuration, especially between the iterations 3 and 4, where the error drops by at least 3 orders of magnitudes. This tremendous result is likely due to the specificity

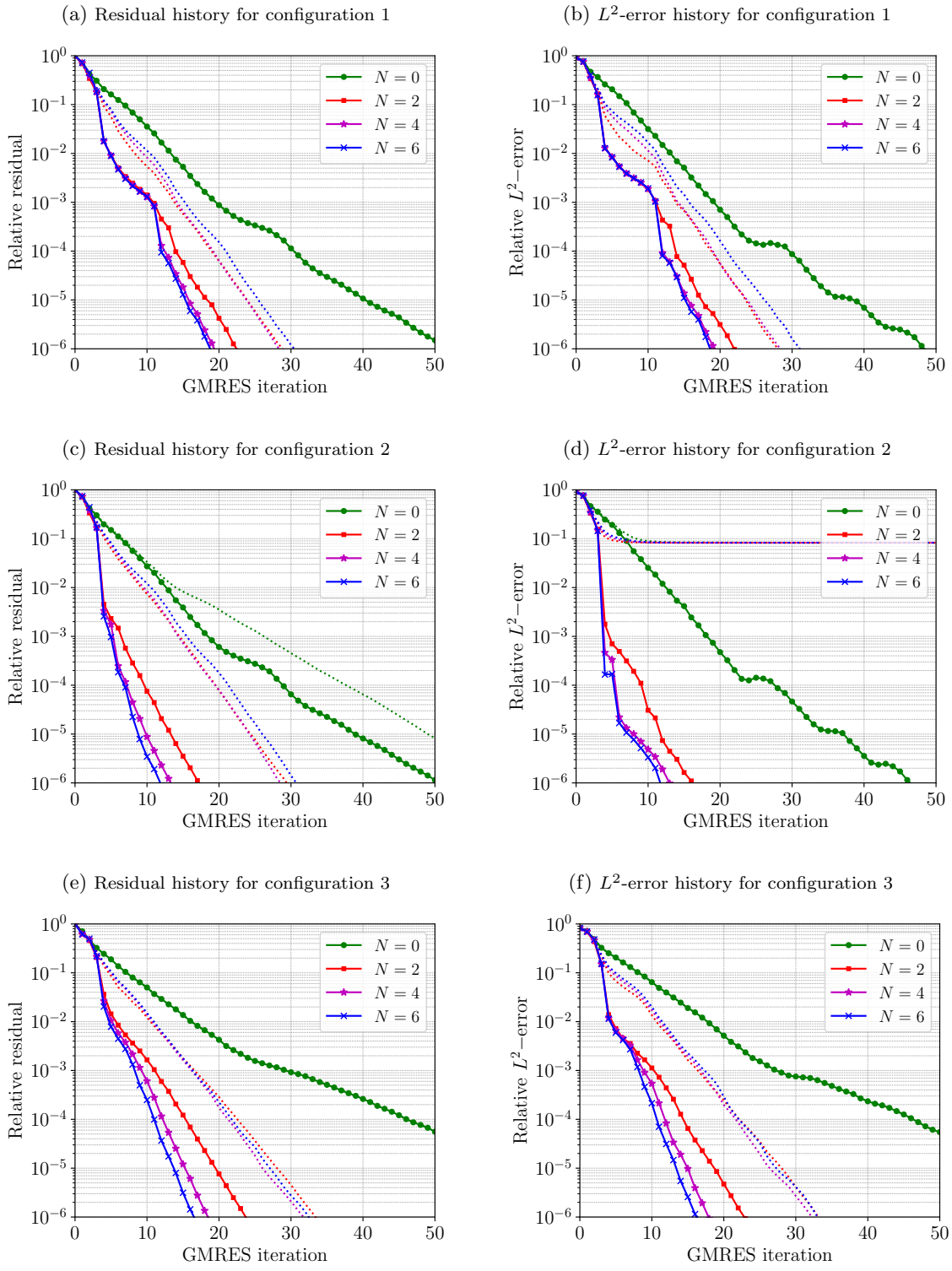

Figure 5: Evolution of relative residual *(left)* and relative L^2-error *(right)* in the course of the GMRES iterations for the three configurations represented in Figure 4. HABC-based transmission conditions with $N = 0, 2, 4, 6$ auxiliary fields and $\phi = 0.3\pi$ are used. The dotted lines correspond to the results obtained when the cross-point treatment is not used. Handling the cross-point procedure is represented by continuous lines.

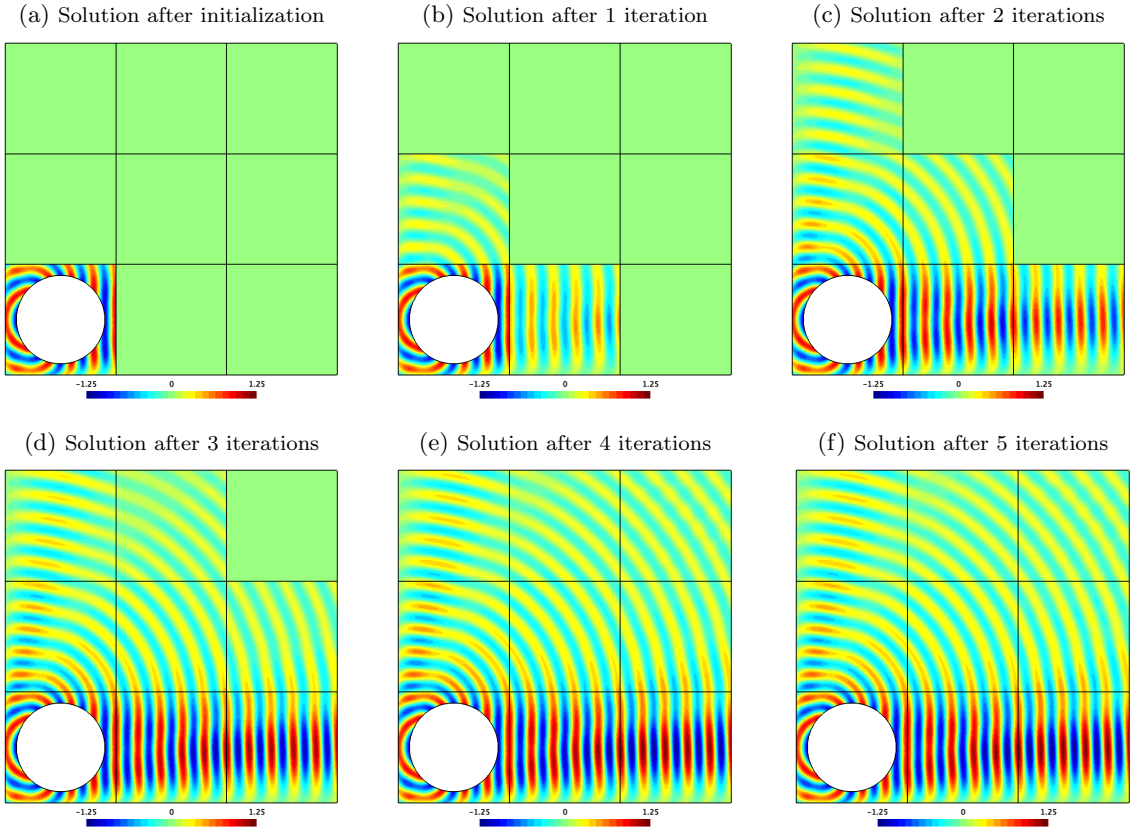

Figure 6: Evolution of the solution during the GMRES iterations for configuration 1 and the HABC-based transmission condition with $N = 4$ and $\phi = 0.3\pi$. The first picture is obtained after initialization of the right-hand side of the transmission system.

of the benchmark: the exact scattering solution verifies the exact free-space boundary condition on the boundary and the interfaces. Since the HABC is used both as exterior BC and transmission condition, the exact behavior of the solution is captured with a few iterations. By contrast, when the basic ABC is used as exterior BC, small waves reflected on the ABC must travel towards the subdomains.

For the third configuration (*i.e.* circular domain with Bayliss–Turkel ABC), both the relative residual and the relative error decrease in all the cases. Again, the decay is faster with the cross-point treatment. Let us highlight that no treatment is used at the boundary cross-points, which corresponds to the junction of interface edges with the exterior boundary (with a Bayliss–Turkel ABC) or the border of the circular scatterer (with an inhomogeneous Dirichlet BC). The method can then be applied to settings with such boundary conditions without any issue.

4.3 Sensitivity to the HABC parameters

The efficiency of the transmission condition depends on the number N of auxiliary fields and the rotating angle ϕ. To study the sensitivity of the convergence to these parameters, we perform the DDM procedure with several values of N and ϕ for the three configurations. The number of GMRES iterations to reach the relative residual 10^{-6} is reported in Figure 7 for the first configuration.

For any given ϕ, increasing the number of auxiliary fields N accelerates the convergence, up to a certain limit, as already mentioned in the previous section. The only exception is for $\phi = 0$. Nevertheless, increasing N leads to a higher computational cost and the amount of data to exchange at the cross-points. It is then advantageous to take the smallest N yielding the best convergence. For practical applications, the optimal N would likely depend on the configuration.

The selection of the parameter ϕ is an important matter, because it accelerates the convergence of

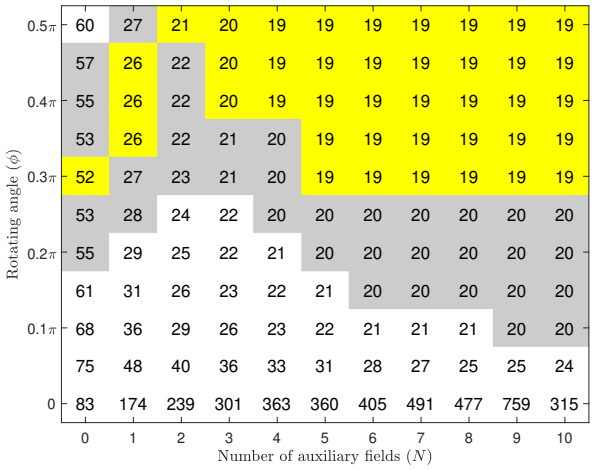

Figure 7: Number of GMRES iterations to reach the relative residual 10^{-6} in configuration 1 for different values of the number of auxiliary fields N and rotating angle ϕ. For each column (*i.e.* each value of N), cells in yellow correspond to the minimal number of iterations, while cells in gray are up to 10% from the minimal number of iterations.

the iterative process at no additional cost. We observe first that the Padé case ($\phi = 0$) gives the worst result in all the cases, and it should be avoided. The optimal value for ϕ, represented for each N by yellow cells in Figure 7, depends on the number N of auxiliary fields. This can make the parameter selection rather tricky. Fortunately, the number of iterations is not very sensitive to ϕ as soon as ϕ is sufficiently large (*i.e.* larger than $\pi/4$ here). The range of the nearly-optimal values of ϕ, represented by the gray zone in Figure 7, is indeed rather wide.

The results for the other configurations lead to similar conclusions. They are not reported here for the sake of conciseness. In the remainder of the paper, we always use $\phi = 0.3\pi$, which is a nearly-optimal value for all the configurations.

4.4 Influence of the wavenumber, the mesh density and the number of subdomains

In this section, we study the sensitivity of the method with respect to the wavenumber κ, the mesh density n_λ and the number of subdomains. High frequency simulations are challenging because they require fine meshes with high mesh densities to avoid the pollution effect. The efficiency of the method for large values of κ and n_λ is therefore an important issue.

Figure 8 shows the number of iterations to reach the relative residual 10^{-6} with respect to κ and n_λ for the various configurations and several values of N. For configurations 1 and 3, the dotted lines correspond to cases where the cross-point treatment is not used. As discussed in Section 4.2, the compatibility is not ensured for configuration 2 if the cross-point treatment is not used.

We first analyze the influence of κ on the convergence. For $N = 0$, the number of iterations increases with respect to κ in all the cases (Figures 8a, 8c and 8e). The increase is very slow for the second configuration, and faster for the third one. For higher values of N, the convergence does not change significantly with κ when the cross-point treatment is used. As already observed, higher values of N accelerate the convergence, and the convergence is slower if the cross-point treatment is not used.

For the first and third configurations, the number of iterations increases with the mesh density n_λ for all the values of N (Figures 8b and 8f). Fortunately, the number of iterations can be kept constant when increasing n_λ by taking N larger: the number of iterations then remains approximately 20 for the first configuration and 17 for the third configuration. Therefore, a convergence independent of the mesh density can be achieved provided that N is sufficiently large. This was already observed in [14] on benchmarks without cross-points treatment. The results are slightly different for the second configuration

(a) Number of iterations *vs* κ for configuration 1

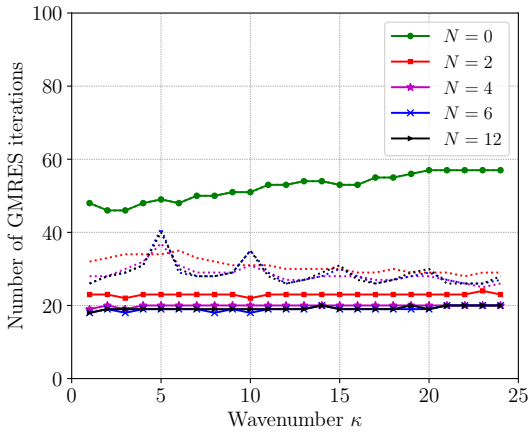

(b) Number of iterations *vs* n_λ for configuration 1

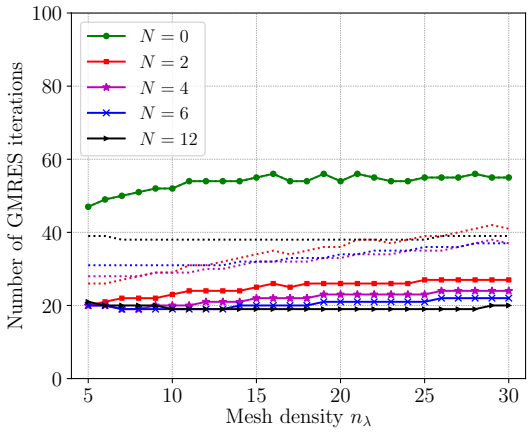

(c) Number of iterations *vs* κ for configuration 2

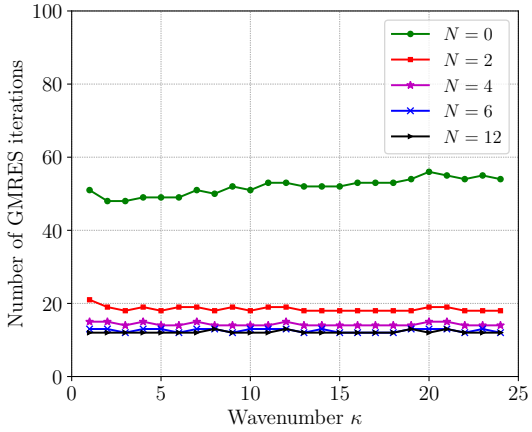

(d) Number of iterations *vs* n_λ for configuration 2

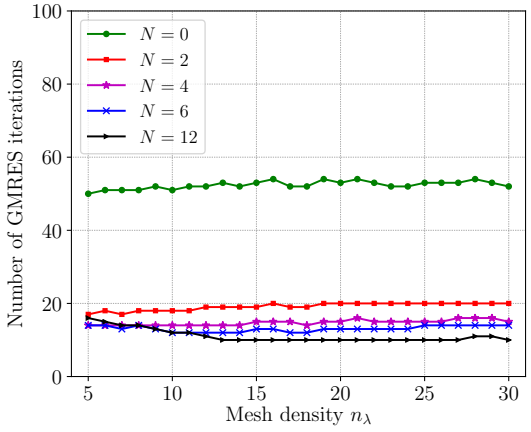

(e) Number of iterations *vs* κ for configuration 3

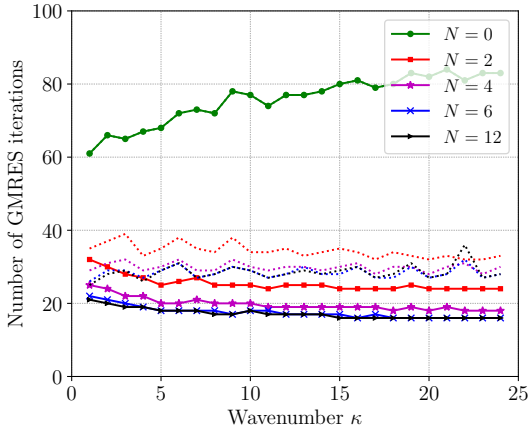

(f) Number of iterations *vs* n_λ for configuration 3

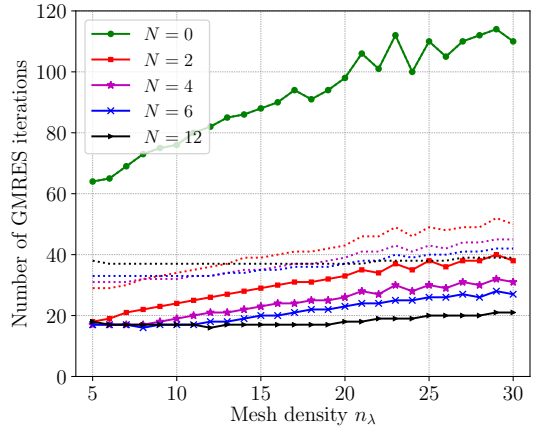

Figure 8: Number of GMRES iterations to reach the relative residual 10^{-6} as a function of the wavenumber κ with a fixed mesh density $n_\lambda = 10$ *(left)* or as a function of the mesh density n_λ with a fixed wavenumber $\kappa = 4\pi$ *(right)* to assert the scaling of the solution with κ and n_λ.

(a) Scaling for configuration 1

(b) Scaling for configuration 3

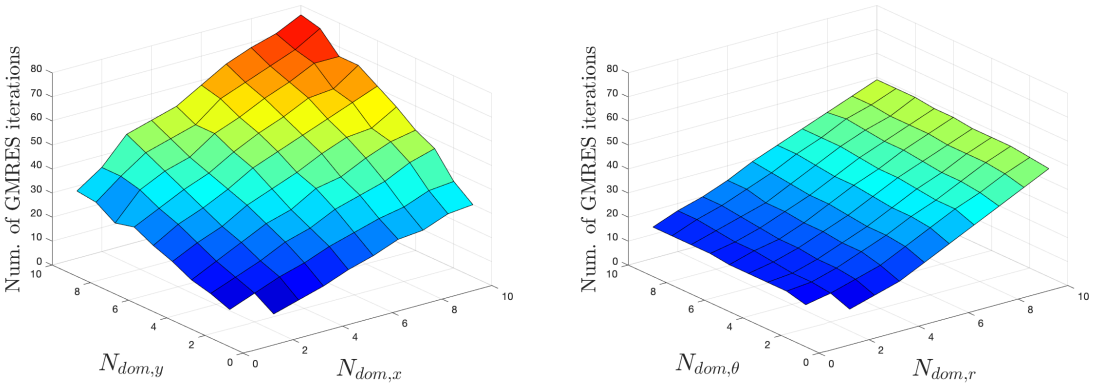

Figure 9: Number of GMRES iterations to reach the relative residual 10^{-6} for different number of subdomains to assert the scaling of the procedure. The size of the main domain increases with the number of subdomains in the x-, y- and r-directions.

(Figure 8d): the number of iterations increases very slowly for $N = 0$ and 2, while it decreases until a plateau for $N = 6$ and 12. The plateau is lower for $N = 12$ than for $N = 6$. This is likely due to the fact that the numerical solution is closer to the exact free-space scattering solution, and that the HABC-based transmission condition is perfectly suited to this specific case.

These results then indicate that the method is well-adapted to high-frequency problems with high density meshes, provided that N is sufficiently large.

Figure 9 shows the evolution of the number of GMRES iterations with respect to the number of subdomains for the first and third configurations. The simulations have been performed with increased numbers of subdomains in the x- and y-directions for the square domain (resp. $N_{\text{dom},x}$ and $N_{\text{dom},y}$) and in the r- and θ-directions for the circular domain (resp. $N_{\text{dom},r}$ and $N_{\text{dom},\theta}$). The size of the domains increases with the number of subdomains: the square domain is $[-1.25, 2.5N_{\text{dom},x} - 1.25] \times [-1.25, 2.5N_{\text{dom},y} - 1.25]$ and the circular domain is $\{(r, \theta) : r \in [1, 1 + N_{\text{dom},r}], \theta \in [0, 2\pi]\}$. The results for the second configuration are similar to those for the first one. They are not reported for the sake of shortness. The strong scaling analysis for the third configuration (*i.e.* increasing the number of subdomains without increasing the size of the domain) also leads to similar results.

The scaling behavior of the method is as expected: the number of iterations increases linearly with the number of subdomains in each direction (Figures 9a and 9b). Indeed, since the transmission of propagating waves from subdomain to subdomain is local with the transmission conditions, a larger number of iterations is required to allow the propagation of waves across a larger number of subdomains. Preconditioning techniques based on sweeps (*e.g.* [35, 69, 72, 76, 77]) and coarse spaces (*e.g.* [4, 10, 25, 37]) allow for global transmissions of information between the subdomains with improved convergences. The combination of our approach with preconditioning techniques is currently under investigation.

4.5 Experiments with non-right angles and heterogeneous media

The proposed DDM is *a priori* suited only to wave propagation in homogeneous media and lattice-type domain partitions with right angles. Indeed, the HABC operator used in the transmission condition is built under the hypothesis of a homogeneous medium, and the compatibility relations used in the cross-point treatment are derived for corners with right angles (see Section 2). Nevertheless, the HABC can be used as a good approximation with smoothly-varying heterogeneous media, since it can represent locally the transmission of waves at the interface (see *e.g.* [60]). The compatibility relations derived for right-angle corners can be used as an approximate treatment with non-right angles [61].

In this section, our approach is tested for configurations where the corner treatment is not exact:

(a) Velocity model

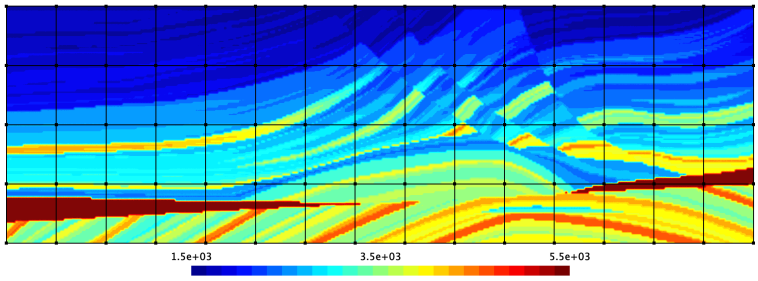

(b) Real part of the numerical solution u

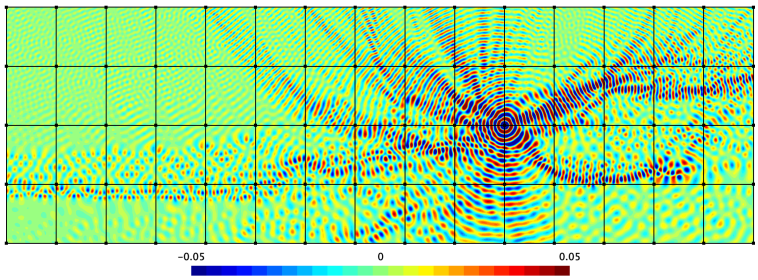

Figure 10: Snapshot of the velocity model (a) and the reference numerical solution (b) for the benchmark with heterogeneous medium.

first, for wave propagation in heterogeneous media (Section 4.5.1) and second for domain partitions with non-right interior angles (Section 4.5.2).

4.5.1 Benchmark with a smoothly varying heterogeneous medium

As a preliminary study to analyze the effectiveness of the method with heterogeneous media, we consider the Marmousi model (Figure 10), a velocity map $c(\mathbf{x})$ that represents a geological structure. This model is frequently used to evaluate modeling and imaging techniques.

The Helmholtz equation with spatially varying wavenumber is solved on the domain,

$$-\Delta u - \kappa(\mathbf{x})^2 u = \delta(\mathbf{x} - \mathbf{x}_{\text{sou}}), \quad \text{on } \Omega,$$

with $k(\mathbf{x}) = 2\pi\nu/c(\mathbf{x})$ and $\Omega = [0, 9192\text{m}] \times [-2904\text{m}, 0]$. The basic ABC is prescribed on all the sides of the domain, and a source point is placed at the position $\mathbf{x}_{\text{sou}}$. The simulations are performed for the frequency $\nu = 30\,\text{s}^{-1}$ and the characteristic mesh size $h \approx 10\text{m}$. The mesh is made of 718 584 triangles and 1 439 613 second-order nodes. Second-degree polynomial basis functions are used.

The domain is partitioned into 4×15 rectangular subdomains. The spatially varying $\kappa(\mathbf{x})$ is used *as is* in the equations of the DDM initially derived for a constant wavenumber. The Dirac source point could be placed on an interior mesh node of any subdomain without difficulty. Here we chose to place the source on an interior cross-point, at coordinates $\mathbf{x}_{\text{sou}} = (6128\text{m}, -1452\text{m})$, in order to demonstrate how such a choice can be combined with the cross-point treatment. To preserve the equivalence with the original problem, the source should be taken into account only in one of the subproblems, which could correspond to any of the four subdomains touching the cross-point. Equivalently, sources could be included in the four subproblems, albeit with their magnitudes determined to sum up to the magnitude of the original source. The treatment of sources on an interface between two subdomains could be handled in a similar way.

Because the parameter analysis performed in Section 4.3 is not longer valid, the HABC-type transmission condition is tested with several numbers of auxiliary fields and rotating angles. The number

Table 1: Number of GMRES iterations to reach the relative residual 10^{-4} for the benchmark with heterogeneous medium.

	$\phi \rightarrow$	0	0.1π	0.2π	0.3π	0.4π	0.5π
No cross-point treatment	$N = 0$	120	94	88	91	103	123
	$N = 1$	>200	56	51	48	48	49
	$N = 2$	>200	51	47	47	47	48
	$N = 3$	>200	51	47	47	47	47
	$N = 4$	>200	51	47	47	47	47
With cross-point treatment	$N = 0$	120	94	88	91	103	123
	$N = 1$	>200	54	49	47	46	48
	$N = 2$	>200	47	45	44	44	44
	$N = 3$	>200	45	43	43	44	44
	$N = 4$	>200	43	43	43	44	44

of GMRES iterations to reach the relative residual 10^{-4} with several values for N and ϕ are shown on Table 1. A preliminary study with coarser meshes, not presented here, has shown that the final relative L^2-error is about 10^{-4} in all the cases. This confirms that the decomposed problems are equivalent to the original problem, despite the heterogeneous medium and the source point on the cross-point.

We observe that using the HABC-based transmission condition (with $N \geq 1$) instead of the basic impedance condition (corresponding to $N = 0$) still accelerates the convergence for every value of $\phi \geq 0.1\pi$. However, the speedup is limited and stagnates rather rapidly when increasing N: using $N = 1$ or 2 is sufficient. This is expected since the HABC operator is not designed for heterogeneous media. Nevertheless, it provides a significant speedup in comparison with the basic impedance condition, with a moderate supplementary computational cost. In addition, the result is not very sensitive to the value of the parameter ϕ: the values in the range $[0.3\pi, 0.5\pi]$ give similar results.

Finally, we observe that, in all the cases, using the cross-point treatment accelerates the convergence. The speedup is rather small, but this is also expected since the issue here is related to the quality of the transmission condition, more than the treatment of the cross-points. Nevertheless, this preliminary study shows that the cross-point treatment remains effective, despite of the smoothly varying heterogeneous medium and the source point at the cross-point. To improve the convergence of the global domain decomposition approach, alternative HABC-based transmission conditions more suited to heterogeneous media should be considered, accelerated with preconditioning techniques, and eventually combined with a cross-point treatment similar to the one proposed here. This approach is currently investigated.

4.5.2 Configurations with distorted partitions

To analyze the method for partitions with non-right angles, we consider the scattering benchmark and the three configurations described in Section 4.1. The partitions are deformed by moving the cross-points, which create acute and obtuse angles, as shown in Figure 11. The points are shifted for the two first configurations (on distances 0.5, 1 and 1.5) and twisted for the third one (by angles 0.1π, 0.2π and 0.3π). In every case, HABC-based transmission conditions with different numbers of auxiliary fields are tested ($N = 0$, 2, 4 and 6 with $\phi = 0.3\pi$). The effect of the cross-point treatment is analyzed by keeping or removing the corresponding terms in the finite element scheme. The terms implemented for the right-angle case are used without modification for non-right angles.

Table 2 shows the number of GMRES iterations to reach the relative residual 10^{-6} for each case. The relative L^2-error (not shown for the sake of shortness) is always close to 10^{-6}, except for the second configuration (*i.e.* square domain with a HABC on the exterior border) without cross-point treatment. As discussed in Section 4.2, the compatibility is not ensured at the boundary cross-points for that case. We have observed that, when using the cross-point treatment, the method converges towards the correct solution, even with an important distortion of the partition. In that case, several interfaces starting from boundary cross-points are not perpendicular to the exterior border.

In nearly all the cases, the number of GMRES iterations increases when the distortion of the partitions is amplified. For the first configuration, the increase is rather small, with and without cross-point treatment. For the two other configurations, the number of iterations increases more rapidly when the

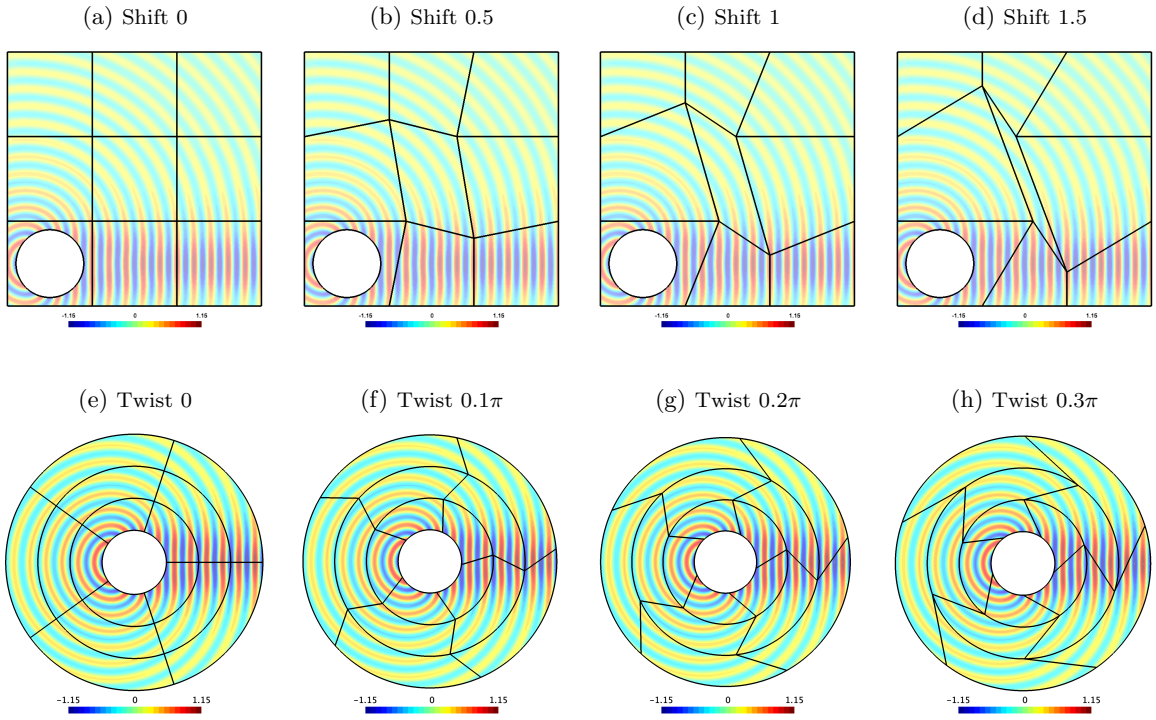

Figure 11: Snapshot of the distorted partitions for the square domain (configurations 1 and 2, Figure 11a-11d) and the circular domain (configuration 3, figures 11e-11h).

Table 2: Number of GMRES iterations to reach the relative residual 10^{-6} for the different configurations with distorted domain partitions. The final relative L^2-error is also approximately 10^{-6} for every case, except for the second configuration without cross-point treatment (results not shown) where the method is not consistent.

		Configuration 1				Configuration 2				Configuration 3			
Shift/Twist →		0	0.5	1	1.5	0	0.5	1	1.5	0	0.1π	0.2π	0.3π
No cross-point treatment	$N=0$	52	55	58	66	-	-	-	-	76	81	85	91
	$N=2$	29	32	32	34	-	-	-	-	34	38	38	38
	$N=4$	29	31	32	33	-	-	-	-	32	34	33	34
	$N=6$	31	32	33	34	-	-	-	-	33	32	31	32
With cross-point treatment	$N=0$	52	55	58	66	51	57	60	67	76	81	85	91
	$N=2$	23	24	25	28	18	22	25	27	24	29	32	34
	$N=4$	20	20	21	24	14	18	20	23	19	24	28	30
	$N=6$	19	19	20	22	12	17	20	21	17	23	26	28

cross-point treatment is used. Nevertheless, in all the cases, using the cross-point treatment accelerates the convergence. The speedup is smaller for the third configuration, but it is still significant. For the most distorted configurations (*i.e.* shift with 1.5 and twist with 0.3π), the smallest numbers of iterations always correspond to the cases with both the largest N and the cross-point treatment. These results show the robustness of the approach with non-right angles.

5 Conclusion

In this work, a non-overlapping DDM with HABC-based transmission operators was considered for the parallel finite-element solution of scattering and wave propagation problems. We presented a suitable way to tackle the cross-point problem for settings with lattice-type domain partitions. In particular, we addressed cases where a Padé-type HABC operator is used for the transmission condition (to accelerate

the convergence of the procedure), for the exterior boundary condition (to improve the accuracy of the solution) or for both conditions.

To handle the cross-points, suitable relations and additional transmission variables were introduced at the points. Numerical results have shown that the convergence rate of the obtained DDM is improved. We systematically studied the way the convergence depends on the tuning parameters of the method as well as the frequency, the mesh refinement and the number of subdomains. Configurations with distorted partitions and heterogeneous media were tested. While the method was conceived for lattice-type partitions with right angles, it also performed very well with partitions having non-right angles. As expected, the efficiency of the approach for configurations with heterogeneous media was not as performant. Current approaches to tackle this problem are based on non-local methods (see *e.g.* [24, 71, 72, 78]) and preconditioners (see *e.g.* [4, 25, 36, 46]).

The extension to the 3D Helmholtz equation can be obtained by adapting the developments of the present paper and the technical details given in [61]. Even if the DDM gains in efficiency thanks to the cross-point treatment, the reported scalability results show that the method is intrinsically dependent on the number of subdomains since the iterated wave field needs to be propagated through the subdomains, translating hence the nonlocal nature of wave-like problems, whatever is the optimized local transmission condition. Furthermore improvements to avoid the problem are currently being developed by using fast sweeping preconditioners [72, 76, 77] and coarse space approximations [4, 25]. Finally, extensions to other time-harmonic wave problems, in particular for electromagnetic [32, 33] and elastic waves [18, 58], are still needed. This is under study but the problem is technically much more complicated.

Acknowledgments

This research was funded in part through the ARC grant for Concerted Research Actions (ARC WAVES 15/19-03), financed by the Wallonia-Brussels Federation of Belgium.

References

[1] X. Antoine and M. Darbas. Generalized combined field integral equations for the iterative solution of the three-dimensional Helmholtz equation. *Mathematical Modelling and Numerical Analysis*, 41(1):147–167, 2007.

[2] X. Antoine, H. Barucq, and A. Bendali. Bayliss–Turkel-like radiation conditions on surfaces of arbitrary shape. *Journal of Mathematical Analysis and Applications*, 229(1):184–211, 1999.

[3] X. Antoine, M. Darbas, and Y. Y. Lu. An improved surface radiation condition for high-frequency acoustic scattering problems. *Computer Methods in Applied Mechanics and Engineering*, 195(33-36):4060–4074, 2006.

[4] A. V. Astaneh and M. N. Guddati. A two-level domain decomposition method with accurate interface conditions for the Helmholtz problem. *International Journal for Numerical Methods in Engineering*, 107(1): 74–90, 2016.

[5] A. Bayliss and E. Turkel. Radiation boundary conditions for wave-like equations. *Communications on Pure and applied Mathematics*, 33(6):707–725, 1980.

[6] J.-D. Benamou and B. Desprès. A domain decomposition method for the Helmholtz equation and related optimal control problems. *Journal of Computational Physics*, 136(1):68–82, 1997.

[7] A. Bendali and Y. Boubendir. Non-overlapping domain decomposition method for a nodal finite element method. *Numerische Mathematik*, 103(4):515–537, 2006.

[8] J.-P. Berenger. A perfectly matched layer for the absorption of electromagnetic waves. *Journal of computational physics*, 114(2):185–200, 1994.

[9] A. Bermúdez, L. Hervella-Nieto, A. Prieto, and R. Rodriguez. An optimal perfectly matched layer with unbounded absorbing function for time-harmonic acoustic scattering problems. *Journal of Computational Physics*, 223(2):469–488, 2007.

[10] M. Bonazzoli, V. Dolean, I. G. Graham, E. A. Spence, and P.-H. Tournier. Two-level preconditioners for the Helmholtz equation. In *International Conference on Domain Decomposition Methods*, pages 139–147. Springer, 2017.

[11] A.-S. Bonnet-Ben Dhia, S. Fliss, and A. Tonnoir. The halfspace matching method: A new method to solve scattering problems in infinite media. *Journal of Computational and Applied Mathematics*, 338:44–68, 2018.

[12] Y. Boubendir and A. Bendali. Dealing with cross-points in a non-overlapping domain decomposition solution of the Helmholtz equation. In *Mathematical and Numerical Aspects of Wave Propagation WAVES 2003*, pages 319–324. Springer, 2003.

[13] Y. Boubendir and D. Midura. Non-overlapping domain decomposition algorithm based on modified transmission conditions for the Helmholtz equation. *Computers & Mathematics with Applications*, 75(6):1900–1911, 2018.

[14] Y. Boubendir, X. Antoine, and C. Geuzaine. A quasi-optimal non-overlapping domain decomposition algorithm for the Helmholtz equation. *Journal of Computational Physics*, 231(2):262–280, 2012.

[15] O. P. Bruno and L. A. Kunyansky. A sparse matrix arithmetic based on H-matrices. Part I: introduction to H-matrices, computing. *Computing*, 62(2):89–108, 1999.

[16] O. P. Bruno and L. A. Kunyansky. A fast, high-order algorithm for the solution of surface scattering problems: basic implementation, tests, and applications. *J. Comput. Phys.*, 169(1):80–110, 2001.

[17] X.-C. Cai and O. B. Widlund. Domain decomposition algorithms for indefinite elliptic problems. *SIAM Journal on Scientific and Statistical Computing*, 13(1):243–258, 1992.

[18] S. Chaillat, M. Darbas, and F. Le Louër. Approximate local Dirichlet-to-Neumann map for three-dimensional time-harmonic elastic waves. *Computer Methods in Applied Mechanics and Engineering*, 297:62–83, 2015.

[19] G. Chen and J. Zhou. *Boundary Element Methods*. Academic Press, New York, 1992.

[20] S. Christiansen and J. Nédélec. Des préconditionneurs pour la résolution numérique des équations intégrales de frontière de l'acoustique. *C.R. Acad. Sci. Paris Sér. I Math.*, 330(7):617–622, 2000.

[21] X. Claeys. A new variant of the optimised Schwarz method for arbitrary non-overlapping subdomain partitions, 2019. http://arxiv.org/abs/1910.05055.

[22] X. Claeys and E. Parolin. Robust treatment of cross points in optimized Schwarz methods, 2020. http://arxiv.org/abs/2003.06657.

[23] F. Collino, S. Ghanemi, and P. Joly. Domain decomposition method for harmonic wave propagation: a general presentation. *Computer methods in applied mechanics and engineering*, 184(2-4):171–211, 2000.

[24] F. Collino, P. Joly, and M. Lecouvez. Exponentially convergent non overlapping domain decomposition methods for the Helmholtz equation. *ESAIM: Mathematical Modelling and Numerical Analysis*, 54(3):775–810, 2020.

[25] L. Conen, V. Dolean, R. Krause, and F. Nataf. A coarse space for heterogeneous Helmholtz problems based on the Dirichlet-to-Neumann operator. *Journal of Computational and Applied Mathematics*, 271:83–99, 2014.

[26] A. de La Bourdonnaye. Some formulations coupling finite element and integral equation methods for Helmholtz equation and electromagnetism. *Numerische Mathematik*, 69(3):257–268, 1995.

[27] A. de La Bourdonnaye, C. Farhat, A. Macedo, F. Magoules, F.-X. Roux, et al. A non-overlapping domain decomposition method for the exterior Helmholtz problem. *Contemporary Mathematics*, 218:42–66, 1998.

[28] B. Després. Domain decomposition method and the Helmholtz problem. In G. Cohen, L. Halpern, and P. Joly, editors, *Proceedings of the First International Conference on Mathematical and Numerical Aspects of wave Propagation Phenomena (Strasbourg, France)*, pages 44–52. SIAM, 1991.

[29] B. Després, A. Nicolopoulos, and B. Thierry. New transmission conditions for corners and cross-points. In *Proceedings of the 14th International Conference on Mathematical and Numerical Aspects of wave Propagation Phenomena (Vienna, Austria)*, 2019.

[30] V. Dolean, P. Jolivet, and F. Nataf. *An introduction to domain decomposition methods: algorithms, theory, and parallel implementation*, volume 144. SIAM, 2015.

[31] P. Dular, C. Geuzaine, F. Henrotte, and W. Legros. A general environment for the treatment of discrete problems and its application to the finite element method. *IEEE Transactions on Magnetics*, 34(5):3395–3398, 1998.

[32] M. El Bouajaji, X. Antoine, and C. Geuzaine. Approximate local magnetic-to-electric surface operators for time-harmonic Maxwell's equations. *Journal of Computational Physics*, 279:241–260, 2014.

[33] M. El Bouajaji, B. Thierry, X. Antoine, and C. Geuzaine. A quasi-optimal domain decomposition algorithm for the time-harmonic Maxwell's equations. *Journal of Computational Physics*, 294:38–57, 2015.

[34] B. Engquist and A. Majda. Absorbing boundary conditions for numerical simulation of waves. *Proceedings of the National Academy of Sciences*, 74(5):1765–1766, 1977.

[35] B. Engquist and L. Ying. Sweeping preconditioner for the Helmholtz equation: moving perfectly matched layers. *Multiscale Modeling & Simulation*, 9(2):686–710, 2011.

[36] Y. A. Erlangga, C. W. Oosterlee, and C. Vuik. A novel multigrid based preconditioner for heterogeneous Helmholtz problems. *SIAM Journal on Scientific Computing*, 27(4):1471–1492, 2006.

[37] C. Farhat, A. Macedo, and M. Lesoinne. A two-level domain decomposition method for the iterative solution of high frequency exterior Helmholtz problems. *Numerische Mathematik*, 85(2):283–308, 2000.

[38] C. Farhat, A. Macedo, M. Lesoinne, F.-X. Roux, F. Magoulés, and A. de La Bourdonnaie. Two-level domain decomposition methods with Lagrange multipliers for the fast iterative solution of acoustic scattering problems. *Computer Methods in Applied Mechanics and Engineering*, 184(2-4):213–239, 2000.

[39] C. Farhat, P. Avery, R. Tezaur, and J. Li. FETI-DPH: a dual-primal domain decomposition method for acoustic scattering. *Journal of Computational Acoustics*, 13(03):499–524, 2005.

[40] M. Gander, F. Magoules, and F. Nataf. Optimized Schwarz methods without overlap for the Helmholtz equation. *SIAM Journal on Scientific Computing*, 24(1):38–60, 2002.

[41] M. J. Gander and F. Kwok. Best Robin parameters for optimized Schwarz methods at cross points. *SIAM Journal on Scientific Computing*, 34(4):A1849–A1879, 2012.

[42] M. J. Gander and F. Kwok. On the applicability of Lions' energy estimates in the analysis of discrete optimized Schwarz methods with cross points. In *Domain Decomposition Methods in Science and Engineering XX*, pages 475–483. Springer, 2013.

[43] M. J. Gander and K. Santugini. Cross-points in domain decomposition methods with a finite element discretization. *Electronic Transactions on Numerical Analysis*, 45:219–240, 2016.

[44] M. J. Gander and H. Zhang. Optimized Schwarz methods with overlap for the Helmholtz equation. *SIAM Journal on Scientific Computing*, 38(5):A3195–A3219, 2016.

[45] M. J. Gander and H. Zhang. A class of iterative solvers for the Helmholtz equation: Factorizations, sweeping preconditioners, source transfer, single layer potentials, polarized traces, and optimized Schwarz methods. *SIAM Review*, 61(1):3–76, 2019.

[46] M. Ganesh and C. Morgenstern. High-order FEM domain decomposition models for high-frequency wave propagation in heterogeneous media. *Computers & Mathematics with Applications*, 75(6):1961–1972, 2018.

[47] C. Geuzaine and J.-F. Remacle. Gmsh: A 3-D finite element mesh generator with built-in pre-and post-processing facilities. *International journal for numerical methods in engineering*, 79(11):1309–1331, 2009.

[48] D. Givoli. Non-reflecting boundary conditions. *Journal of computational physics*, 94(1):1–29, 1991.

[49] I. Graham, E. Spence, and E. Vainikko. Domain decomposition preconditioning for high-frequency Helmholtz problems with absorption. *Mathematics of Computation*, 86(307):2089–2127, 2017.

[50] T. Hagstrom, R. P. Tewarson, and A. Jazcilevich. Numerical experiments on a domain decomposition algorithm for nonlinear elliptic boundary value problems. *Applied Mathematics Letters*, 1(3):299–302, 1988.

[51] R. Kechroud, X. Antoine, and A. Soulaimani. Numerical accuracy of a Padé-type non-reflecting boundary condition for the finite element solution of acoustic scattering problems at high-frequency. *International Journal for Numerical Methods in Engineering*, 64(10):1275–1302, 2005.

[52] S. Kim and H. Zhang. Optimized Schwarz method with complete radiation transmission conditions for the Helmholtz equation in waveguides. *SIAM Journal on Numerical Analysis*, 53(3):1537–1558, 2015.

[53] J.-H. Kimn and M. Sarkis. Restricted overlapping balancing domain decomposition methods and restricted coarse problems for the Helmholtz problem. *Computer Methods in Applied Mechanics and Engineering*, 196 (8):1507–1514, 2007.

[54] M. Lecouvez, B. Stupfel, P. Joly, and F. Collino. Quasi-local transmission conditions for non-overlapping domain decomposition methods for the Helmholtz equation. *Comptes Rendus Physique*, 15(5):403–414, 2014.

[55] W. Leng and L. Ju. An additive overlapping domain decomposition method for the Helmholtz equation. *SIAM Journal on Scientific Computing*, 41(2):A1252–A1277, 2019.

[56] S. Loisel. Condition number estimates for the nonoverlapping optimized Schwarz method and the 2-Lagrange multiplier method for general domains and cross points. *SIAM Journal on Numerical Analysis*, 51(6):3062–3083, 2013.

[57] N. Marsic and H. D. Gersem. Convergence of optimized non-overlapping Schwarz method for Helmholtz problems in closed domains, 2020. Preprint arXiv 2001.01502.

[58] V. Mattesi, M. Darbas, and C. Geuzaine. A high-order absorbing boundary condition for 2D time-harmonic elastodynamic scattering problems. *Computers & Mathematics with Applications*, 77(6):1703–1721, 2019.

[59] F. A. Milinazzo, C. A. Zala, and G. H. Brooke. Rational square-root approximations for parabolic equation algorithms. *The Journal of the Acoustical Society of America*, 101(2):760–766, 1997.

[60] A. Modave, A. Atle, J. Chan, and T. Warburton. A GPU-accelerated nodal discontinuous Galerkin method with high-order absorbing boundary conditions and corner/edge compatibility. *International Journal for Numerical Methods in Engineering*, 112(11):1659–1686, 2017.

[61] A. Modave, C. Geuzaine, and X. Antoine. Corner treatments for high-order local absorbing boundary conditions in high-frequency acoustic scattering. *Journal of Computational Physics*, 401:109029, 2020.

[62] F. Nataf, F. Rogier, and E. de Sturler. Optimal interface conditions for domain decomposition methods. *CMAP (Ecole Polytechnique)*, 301:1–18, 1994.

[63] J. Nédélec. *Acoustic and Electromagnetic Equations. Integral Representations for Harmonic Problems*. Applied Mathematical Sciences. Springer, 2001.

[64] A. Nicolopoulos. *Formulations variationnelles d'équations de Maxwell résonantes et problèmes aux coins en propagation d'ondes*. PhD thesis, Sorbonne Université, 2019.

[65] A. Piacentini and N. Rosa. An improved domain decomposition method for the 3D Helmholtz equation.

Computer Methods in Applied Mechanics and Engineering, 162(1-4):113–124, 1998.

[66] A. Quarteroni and A. Valli. *Domain decomposition methods for partial differential equations*. Numerical Mathematics and Scientific Computation. The Clarendon Press, Oxford University Press, New York, 1999.

[67] V. Rokhlin. Rapid solution of integral equations of scattering theory in two dimensions. *J. Comput. Phys.*, 86(2):414–439, 1990.

[68] A. Schädle and L. Zschiedrich. Additive Schwarz method for scattering problems using the PML method at interfaces. In *Domain Decomposition Methods in Science and Engineering XVI*, pages 205–212. Springer, 2007.

[69] C. C. Stolk. A rapidly converging domain decomposition method for the Helmholtz equation. *Journal of Computational Physics*, 241:240–252, 2013.

[70] C. C. Stolk. An improved sweeping domain decomposition preconditioner for the Helmholtz equation. *Advances in Computational Mathematics*, 43(1):45–76, 2017.

[71] B. Stupfel. Improved transmission conditions for a one-dimensional domain decomposition method applied to the solution of the Helmholtz equation. *Journal of Computational Physics*, 229(3):851–874, 2010.

[72] M. Taus, L. Zepeda-Núñez, R. J. Hewett, and L. Demanet. L-Sweeps: A scalable, parallel preconditioner for the high-frequency Helmholtz equation, 2019. http://arxiv.org/abs/1909.01467.

[73] B. Thierry, A. Vion, S. Tournier, M. El Bouajaji, D. Colignon, N. Marsic, X. Antoine, and C. Geuzaine. GetDDM: an open framework for testing optimized Schwarz methods for time-harmonic wave problems. *Computer Physics Communications*, 203:309–330, 2016.

[74] A. Toselli and O. Widlund. *Domain decomposition methods-algorithms and theory*, volume 34. Springer Science & Business Media, 2006.

[75] E. Turkel and A. Yefet. Absorbing PML boundary layers for wave-like equations. *Applied Numerical Mathematics*, 27(4):533–557, 1998.

[76] A. Vion and C. Geuzaine. Double sweep preconditioner for optimized Schwarz methods applied to the Helmholtz problem. *Journal of Computational Physics*, 266:171–190, 2014.

[77] A. Vion and C. Geuzaine. Improved sweeping preconditioners for domain decomposition algorithms applied to time-harmonic Helmholtz and Maxwell problems. *ESAIM: Proceedings and Surveys*, 61:93–111, 2018.

[78] L. Zepeda-Núñez and L. Demanet. The method of polarized traces for the 2D Helmholtz equation. *Journal of Computational Physics*, 308:347–388, 2016.